Sudhanshu Tripathi\*, Rekha Agarwal and Devraj Singh

# Size-Dependent Ultrasonic and Thermophysical Properties of Indium Phosphide Nanowires

https://doi.org/10.1515/zna-2019-0351 Received November 27, 2019; accepted January 30, 2020; previously published online March 7, 2020

**Abstract:** The present work explores the diameter- and temperature-dependent ultrasonic characterization of wurtzite indium phosphide nanowires (WZ-InP-NWs) using a theoretical model based on the ultrasonic nondestructive evaluation (NDE) technique. Initially, the second- and third-order elastic constants (SOECs and TOECs) were computed using the Lennard-Jones potential model, considering the interactions up to the second nearest neighbours. Simultaneously, the mechanical parameters (Young's modulus, shear modulus, elastic anisotropy factor, bulk modulus, Pugh's ratio and Poisson's ratio) were also estimated. Finally, the thermophysical properties and ultrasonic parameters (velocity and attenuation) of the InP-NWs were determined using the computed quantities. The obtained elastic/mechnical properties of the InP-NWs were also analyzed to explore the mechanical behaviors. The correlations between temperature-/sizedependent ultrasonic attenuation and the thermophysical properties were established. The ultrasonic attenuation was observed to be the third-order polynomial function of the diameter/temperature for the InP nanowire.

**Keywords:** Elastic Constants; Indium Phosphide Nanowires; Thermal Conductivity; Ultrasonic Attenuation.

**PACS No.:** 43.35.Fj; 62.20. Mk; 62.65.+k; 74.25. Ld.

**Rekha Agarwal:** Department of Electronics and Communication Engineering, Amity School of Engineering and Technology, Noida 201313, India

**Devraj Singh:** Department of Physics, Prof. Rajendra Singh (Rajju Bhaiya) Institute of Physical Sciences for Study and Research, V.B.S.P. University, Jaunpur 222003, India

### 1 Introduction

Rigorous investigations carried out in the last decade have exhibited the applicability of indium phosphide (InP) at the nanoscale. InP is a III-V group semiconductor material that exists in the wurtzite (WZ) and zinc blende (ZB) crystalline forms at room temperature (300 K) [1-3]. The observation of the WZ phase in the crystal lattice of the InP nanostructure is an important finding that cannot be found at the bulk scale, where the zinc blende form is pervasive. Recent investigations have shown that the suitability of the InP nanowires (InP-NWs) for high-speed digital circuits, opto-electronic devices, and high-frequency and high-power electronics applications due to its high electron mobility, high degree of covalent bonding, large excitation diameter and less ionic characteristics in comparison to the I-VII and II-VI semiconductors [4-7]. Figure 1 shows the hexagonal WZ structure of the InP nanowire and its cross-sectional view. The figure clearly indicates that very few InP atoms are lying on the surface of nanowire in comparison to the volume.

The experimental study of mechanical and fracture mechanisms in the InP-NWs shows that the fracture strain of the InP-NWs is like that of the ZnO-NWs but lesser than that of the GaAs-NWs. A density function theory (DFT)-based investigation on InP has shown that pressure variation can also affect the chemical bonding leading to modification in crystal structure and physical properties of InP [3]. The two forms (ZB and WZ) of the InP-NWs structure differ due to stacking along <111>/<001> growth directions [8]. The band gap difference between WZ- and ZB-InP-NWs can be described as  $\Delta E_g = 0.79/d$  and  $\Delta E_g =$  $0.88/d^{1.32}$ , respectively, as a function of diameter (d) [9]. The study on piezoelectric and elastic properties along the <111>/<001> directions of ZB- and WZ-structured NWs with three different forms of hetero-structures reveals that the piezoelectric field along the unique axis of nanowires is more prominent in the WZ crystalline form [10]. The variations in the shear strains in both forms of the nanowires' crystalline structures influence their mechanical properties. However, it has been reported that the principal shear strain is independent of crystalline structure variations and that the piezoelectric field/piezoelectric potential of the nanowires depends on the crystalline structures [10].

<sup>\*</sup>Corresponding author: Sudhanshu Tripathi, University School of Information Communication and Technology, Guru Gobind Singh Indraprastha University, Dwarka, New Delhi 110078, India; and Department of Instrumentation and Control Engineering, Amity School of Engineering and Technology, Noida 201313, India, E-mail: tripathisudhanshu@gmail.com. https://orcid.org/0000-0001-8865-7987

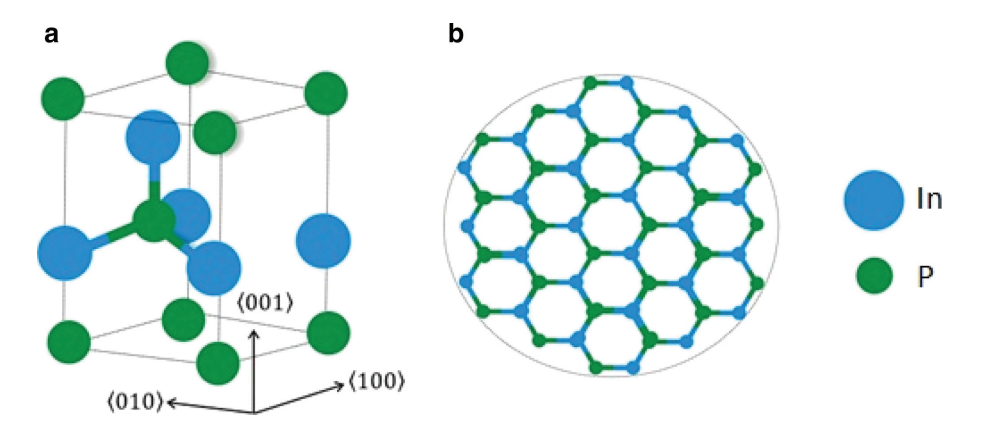


Figure 1: (a) Wurtzite-InP unit cell (b) Cross-sectional view of the InP-NWs.

The structural and phase transition studies on InP-NWs show that the crystal structure transition depends on growth conditions. The surface energy is the key aspect to understanding the phenomena of transition between the WZ- and ZB- structures of InP-NWs [11]. The electronic, structural and mechanical studies of InP- and InAs-NWs reveal the impact of nanowire diameter variation on the physical properties and their variations from the bulk values.

The electron effective masses and band gap of nanowires vary inversely with their diameters [12]. Luca et al. [13] discussed in detail the growth process, optical, structural and electronic characteristics of WZ-InP-NWs using the optical and magneto-optical spectroscopy method. A previous study also reported that the crystal structure modification leads to changes in the transport properties of nanowires, which are essential in estimating the values of fundamental parameters (thermal and electrical conductivity, carrier mobility, quantum confinement etc.) in nanowire-based devices. Recently, the thermoelectric properties of InAs/InP-NWs have been studied in a high-temperature regime [14]. They have estimated the electronic figure of merit for comparative performance study of electronic properties of thermoelectric devices. Göransson et al. [15] demonstrated the measurement of strain and band gap in InAs-InP core shell nanowires for the WZ-crystal phase. Both the size (diameter) and temperature affect the thermophysical properties of the material. The essential characterization of the III-V group semiconductors with size and temperature is required for enhancing their applicability in device applications.

To the best of the authors' knowledge, no evidence has been presented concerning an ultrasonic study of InP-NWs in the available literature. Therefore, the present work includes the determination of the mechanical, thermal and ultrasonic properties of the nanostructured WZ-InP-NWs. The work is divided in two phases. In the first phase,

we estimated the elastic and mechanical behaviors of the WZ-InP-NWs at room temperature using the Lennard-Jones potential model. In the second phase, the obtained values of the higher order elastic constants of the InP-NWs are applied to estimate the ultrasonic and thermophysical properties of the WZ-InP-NWs under varying temperatures (100 K–500 K) and diameters (0.81 nm–5 nm).

# 2 Theory

The higher order elastic constants of the WZ-InP-NWs can be determined either by the stress-strain relationship or by the evaluation of elastic energy density in terms of strain. The second-order elastic constants (SOECSs) and third-order elastic constants (TOECs) are the functions of elastic energy density (F), which depend on the Lennard-Jones Potential and the lattice parameters under many body interaction potential model approach [16]. The expressions for SOECs ( $C_{jk}$ ) and TOECs ( $C_{jkl}$ ) for the WZ structured materials can be obtained with the help of the following equations [17]:

$$C_{jk} = \frac{\partial^2 F}{\partial \zeta_j \partial \zeta_k}; \qquad j, k = 1, 2.....6$$

$$C_{jkl} = \frac{\partial^3 F}{\partial \zeta_l \partial \zeta_k \partial \zeta_l}; \qquad j, k, l = 1, 2.....6$$
(1)

where  $\zeta_i = \zeta_{jk}(j, k = x, y, z; i = 1, 2 \dots 6)$  represents the strain tensor component. Using many body interaction potentials within the symmetric and equilibrium conditions, (1) provides the formulations of SOECs and TOECs. The formulations of SOECs and TOECs for the WZ structured materials have already been reported in the literature [16–18]. Relying on the knowledge of SOECs, the mechanical stability of hexagonal structured material can

be analyzed on the basis of the following Born's stability criterion [19]:

$$C_{44} > 0; C_{66} > 0; C_{11} > |C_{12}|;$$
  
 $(C_{11} + C_{12})C_{13} > 2C_{13}^{2}$  (2)

The mechanical parameters of solids can be evaluated using the elastic constants. The strength, stability and materials' behavior under the influence of various forces acting on it, can be investigated with its mechanical properties. The Young's modulus Y, shear modulus G, elastic anisotropy factor  $EA_F$ , bulk modulus G, Pugh's ratio G and Poisson's ratio G are well-related to the SOECs. The expressions for these parameters are given below [20–22]:

$$B = 0.5 (B_{\text{Voigt}} + B_{\text{Reuss}});$$

$$G = 0.5 (G_{\text{Voigt}} + G_{\text{Reuss}});$$

$$\sigma = \left( (3G)^{-1} - (2B)^{-1} \right) / \left( (6G)^{-1} - (2B)^{-1} \right)$$

$$Y = \left\{ (3G)^{-1} + (9B)^{-1} \right\}^{-1};$$

$$P = \frac{B}{G};$$

$$EA_F = C_{44}(C_{11} + 2C_{13} + C_{33}) / \left( C_{11}C_{33} - C_{13}^2 \right);$$

$$B_{\text{Reuss}} = C^2 / N$$

$$B_{\text{Voigt}} = 9^{-1} \left( 2(C_{11} + C_{12}) + 4C_{13} + C_{33} \right);$$

$$C^2 = C_{33}(C_{11} + C_{12}) - 2C_{13}^2;$$

$$N = (C_{12} + C_{11} + 2C_{33} - 4C_{13})$$

Here, quantities B and G are the average values of the bulk and shear modulus, respectively, under Voigt, Reuss and Hill's approximation. The elastic anisotropy factor provides information about the anisotropic behavior of the material, whereas the Pugh's ratio defines the ductility or brittleness of the material [21]. The ultrasonic wave velocity is another important property of the material, and this has been used to analyze the crystallographic texture of InP-NWs as it depends on the stiffness parameter, angle of propagation ( $\theta$ ) with unique axis and material density ( $\rho$ ). Debye theory describes the Debye average velocity ( $V_D$ ) in terms of different modes of wave propagation, and is an important fact in accessing the information about the thermal relaxation mechanism and Debye temperature ( $\theta_D$ ) of the material.  $V_D$  is defined as [23]

$$V_D = \left[ \frac{1}{3} \left( \frac{1}{V_L^3} + \frac{1}{V_{s_1}^3} + \frac{1}{V_{s_2}^3} \right) \right]^{-1/3} \tag{4}$$

where  $V_I$  (I=L, S1, S2) signifies the ultrasonic velocity. Here, the subscripts L, S1 and S2 represent the longitudinal, quasi-shear and shear modes of the ultrasonic wave, respectively. The ultrasonic velocities at different orientations can be obtained with the expressions given in the literature [18, 20]. The ultrasonic attenuation ( $\alpha$ ) is also an important ultrasonic parameter that is needed for the characterization of materials. This can be obtained with the following expression [24]:

$$(\alpha/\upsilon^{2})_{\text{Total}} = (\alpha/\upsilon^{2})_{TE} + (\alpha/\upsilon^{2})_{\text{Long,Akh}} + (\alpha/\upsilon^{2})_{\text{Shear,Akh}}$$
(5)

where v is the frequency of ultrasonic wave; the quantities  $(\alpha/v^2)_{TE}$ ,  $(\alpha/v^2)_{\text{Long.Akh}}$  and  $(\alpha/v^2)_{\text{Shear.Akh}}$  represent different factors contributing to total ultrasonic attenuation;  $(\alpha/v^2)_{TE}$  is the ultrasonic attenuation due to thermoelastic loss; and  $(\alpha/v^2)_{\text{Long.Akh}}$  and  $(\alpha/v^2)_{\text{Shear.Akh}}$  are the Akhieser type losses. The thermoelastic loss occurs due to the heat exchange between the two different temperature regions created by longitudinal ultrasonic wave propagation [24, 25]. The thermoelastic loss is expressed as

$$\left(\alpha/\upsilon^2\right)_{TE} = \frac{4\pi^2 \kappa T \left(\gamma_i^j\right)^2}{2\rho V_L^5} \tag{6}$$

where  $\kappa$  is thermal conductivity and  $\langle \gamma_i^j \rangle$  is the Grüneisen parameter. The diameter/temperature dependent  $\kappa$  of the InP-NWs have been previously reported in the literature [26]. The Grüneisen parameter can be estimated using the knowledge of SOECs and TOECs [27]. The Akhieser loss  $((\alpha)_{Akh})$  is caused by the phonon-phonon interaction mechanism, which has a prominent effect on the ultrasonic attenuation in solids and is given as [22]

$$\left(\alpha/\upsilon^2\right)_{Akh} = \frac{4\pi^2 \tau (DE_0/3)}{2\rho V^3 \left(1 + \omega^2 \tau^2\right)} \tag{7}$$

where  $\omega=2\pi\upsilon$ . The acoustic energy is transformed to thermal energy during the wave propagation and is measured in terms of acoustic coupling constant D, which is defined as

$$D = 9\left\langle \left(\gamma_i^j\right)^2\right\rangle - 3\left\langle \gamma_i^j\right\rangle^2 \frac{C_V T}{E_0} \tag{8}$$

where  $C_V$  is specific heat per unit volume and  $E_0$  is the thermal energy density. The quantities  $C_V$  and  $E_0$  can be obtained by the use of the  $\theta_D/T$  tables of the AIP Handbook [28]. The thermal relaxation time  $(\tau)$  measures the re-establishment time for thermal phonons after the

propagation of the ultrasonic wave through the material, which is well-related to the specific heat per unit volume, thermal conductivity and Debye average velocity [23, 28]. The computation of  $\tau$  uses the following equation:

$$\tau = 0.5\tau_1 = \tau_s = 3\kappa/C_V V_D^2 \tag{9}$$

# 3 Results and Discussion

The SOECs and TOECs for the InP-nanowires have been evaluated using axial ratio (p), the Lennard-Jones parameter  $(b_0)$  and lattice parameters (a and c) at 300 K. The values of the lattice parameters have been taken from the literature [29]. The axial ratio of the InP nanowire at 300 K is 1.6414. The value of the Lennard-Jones parameter, which is  $1.3284 \times 10^{-63}$  erg-cm<sup>7</sup>, has been found in the equilibrium condition. Table 1 depicts the calculated SOECs and TOECs of the InP-NWs at 300 K. The obtained values of the SOECs are in good agreement with the reported theoretical/experimental values for the nano-sized InPs [3, 30–32]. The obtained values of the TOECs in the present work for the WZ-InP-NWs are all negative. The negative values of the TOECs indicate that the vibrational frequencies increase under stress, which in turn, increase the strain energy. The TOECs values correspond to the anisotropy of the longitudinal modes ( $C_{111}$ ,  $C_{222}$  and  $C_{333}$ ) that have higher values than their shear moduli ( $C_{144}$ ,  $C_{155}$ ). Hence, the external stimuli will be more effective on the longitudinal mode than the shear mode. Given that  $C_{111} > C_{333}$ ; thus, the anisotropy along the ab-plane of the InP-NWs is more prominent than that along the c-axis. Moreover, the linear compressibility along the c-axis will be much lower than that along the ab-axis. The negative values of the TOECs have also been reported for similar WZ structured semiconducting nanowires [33, 34]. Hence, our theory for the calculation of the higher order elastic constants of the InP-NWs is justified.

The Born's stability criterion for the WZ structured materials, as given in (2), has been satisfied by the computed values of the elastic constants for the InP-NWs, thus indicating the mechanical stability of the InP-NWs. The dynamical and mechanical characteristics of the InP-NWs with respect to the types of forces applied to them can be determined using the elastic constants. The calculated values of the SOECs have been utilized to compute the mechanical parameters of the InP-NWs using (3). The calculated values of the Poisson ratio, shear modulus, bulk modulus and Young modulus are presented in Table 1. The obtained value of the bulk modulus (73 GPa) is the same as that of the theoretically/experimentally reported values (70–73 GPa) for the chosen InP at the nanoscale [2, 3]. Dunaevskiy et al. [35] have shown that the Young' modulus of the mixed (ZB/WZ) InP-NWs is approximately 40 % less than that of the ZB crystalline InP-NWs. The obtained value of the Young's modulus for the WZ-InP-NWs (124.1 GPa) lies within the range of the theoretically estimated values of 120  $\pm$  10 GPa and the experimentally reported values of 130  $\pm$  30 GPa. The Pugh's ratio (P) obtained for the InP-NWs at room temperature is above 1.75, which indicates the ductile behavior of the WZ-InP-NWs. The obtained elastic anisotropy factor is 0.86, which is far away from 1, thus indicating the anisotropic characteristics of the interaction forces among the InP atoms. Although the lattice parameters of the crystalline material are temperature-/ size-dependent, the variation in lattice parameters is negligibly small in the chosen range of the temperature/ diameter to affect the elastic/mechanical properties of the InP-NWs. Therefore, the computed elastic constants are assumed to be same in the chosen range of temperature and diameter variation of InP nanowire.

Table 1: The elastic constants and mechanical parameters of the InP-NWs at 300 K.

SOECs and mechanical parameters	Present work	Ref. [3] <sup>a</sup>	Ref. [30] <sup>b</sup>	Ref. [31] <sup>c</sup>	Ref. [32] <sup>d</sup>	TOECs in (GPa)	Present work
C <sub>11</sub> (GPa)	114.4	99.9	116.7	131.1	101.1	C <sub>111</sub>	-1865.6
$C_{12}(GPa)$	56.1	56.1	50.9	51.3	56.1	C <sub>112</sub>	-295.7
$C_{13}(GPa)$	49.2	-	38.2	38.6	-	C <sub>113</sub>	-63.1
C33(GPa)	119.3	-	135.9	143.8	_	C <sub>123</sub>	-80.2
$C_{44}(GPa)$	29.5	43.8	27.0	32.1	45.6	C <sub>133</sub>	-403.2
C <sub>66</sub> (GPa)	29.1	-	32.9	-	_	C <sub>344</sub>	-378.0
B(GPa)	73.0	70.7	-	-	_	C <sub>144</sub>	-93.5
G(GPa)	30.4	33.2	-	-	_	C <sub>155</sub>	-62.3
Y(GPa)	124.1	113.9	-	-	112.7	$C_{222}$	-1476.1
σ	0.31	0.25	_	_	0.24	C333	-1527.8

 $<sup>^</sup>a$  Ref. [3],  $^b$  Ref. [30]: for the InP-NWs;  $^{c,d}$  Refs. [31, 32]: for the InP at the bulk scale.

The ultrasonic wave velocity in semiconductors depends on stiffness parameters, density and propagation angle. Using the higher order elastic constants, the three types of ultrasonic velocities (longitudinal wave velocity, quasi-shear wave velocity and shear wave velocity) and their angle-dependent characteristics have been obtained at 300 K. Finally, the Debye average velocity has been computed using (4). The obtained values of the ultrasonic velocities at 300 K are depicted in Table 2. Figure 2 presents the angle-dependent variation of the ultrasonic wave velocities and the Debye average velocity at 300 K.

As shown in Figure 2, the longitudinal ultrasonic wave velocity has maxima at 55° and the quasi-shear wave velocity has minima at 45°, whereas the shear wave velocity decreases with the increase in propagation angle from the unique axis of the crystal. Figure 2 also clearly shows that the Debye average velocity has maxima for ultrasonic wave propagation at 50° with a unique axis. This uniqueness in  $V_D$  is due to the combined behavior of the constituent velocities. The longitudinal velocity and shear wave velocity for the InP-NWs at room temperature are  $4.99 \times 10^3 \text{ ms}^{-1}$  and  $2.78 \times 10^3 \text{ ms}^{-1}$ , respectively, which are in good agreement with the existing values of the InP in the literature [32, 36, 37]. The ultrasonic velocities of InP-NWs are found to be approximately the same as for bulk InP due to the very insignificant variation in the lattice parameter at the nanoscale. The obtained pattern of ultrasonic velocities for the InP-NWs have been found similar to other hcp/WZ structured materials [16, 33, 34, 38]. Thus, our ultrasonic velocity evaluation of the WZ-InP-NWs seems correct.

The thermophysical quantities, the specific heat per unit volume  $C_V$ , the crystal energy density  $E_0$  and the acoustic coupling constants ( $D_L$  and  $D_S$ ) have all been evaluated at 300 K using  $V_D$  described in (4) and the  $\theta_D/T$  tables of the AIP Handbook [28, 39]. The obtained values of  $C_V$ ,  $E_0$ ,  $\theta_D$ ,  $D_L$  and  $D_S$  with ultrasonic velocities at 300 K are shown in Table 2. The values of  $D_S$  are found to be constant within the chosen range of temperature. The temperature variations of  $C_V$ ,  $E_0$  and  $D_L$  are also depicted in Figure 3.

The work of Dabhi et al. [40] reports that the value of the Debye temperature for InP-NWs is 430 K, which is found very close to the present value (Tab. 2). Thus, the estimated value of  $\theta_D$  is justified. The specific heat of

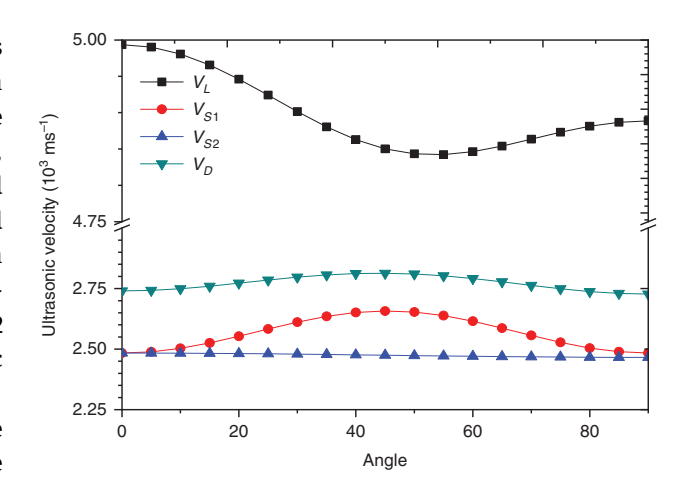


Figure 2: The angle-dependent ultrasonic velocity at 300 K.

InP-NWs has been found to follow the stable characteristics with small dispersion at higher temperature (Fig. 3a). This feature of  $C_V$  is due to stability in the phonon mean free path at a high temperature. Given that the specific heat behavior is found to be in accordance with Debye theory and the literature [40], therefore, the present  $C_V$  is justified. As the increase in vibrational energy with temperature corresponds to enhancement in thermal energy density, thus, quantity  $E_O$  is found to increase with temperature (Fig. 3a). The lower value of  $D_S$  in comparison to  $D_L$  (Tab. 2) indicates that the conversion of acoustical to thermal energy is least for the surface/shear wave for the InP nanowire.

For the determination of the thermal relaxation time and ultrasonic attenuation, the thermal conductivity values ( $\kappa$ ) of the InP-NWs under different temperatures and different diameters have been taken from the literature [26]. The diameter-/temperature-dependent ultrasonic attenuation due to thermoelastic relaxation mechanism  $(\alpha/\upsilon^2)_{TE}$ , Akhieser loss  $(\alpha/\upsilon^2)_{Akh}$  for longitudinal/shear wave and thermal relaxation time  $\tau$  have all been calculated using (6)–(9), respectively. The temperature-dependent  $\tau$ ,  $\kappa$ ,  $(\alpha/\upsilon^2)_{TE}$  and  $(\alpha/\upsilon^2)_{Akh}$  for InP-NWs at the diameters of 1.66 nm and 4.15 nm are given in Table 3. Simultaneously, the variations of  $\tau$  and  $(\alpha/\upsilon^2)_{Total}$  with diameter at 300 K are presented in Figure 4, while the temperature dependencies of  $(\alpha/\upsilon^2)_{Total}$  at the diameters of 1.66 nm and 4.15 nm are depicted in Figure 5.

**Table 2:** The  $C_V$ ,  $E_0$ ,  $D_L$ ,  $D_S$ ,  $V_L$ ,  $V_S$  and  $V_D$  values of the InP-NWs at 300 K up to a diameter of 5 nm.

$C_V$ (10 <sup>6</sup> Jm <sup>-3</sup> K <sup>-1</sup> )	$E_0$ (10 <sup>6</sup> Jm <sup>-3</sup> )	$\theta_D$ (K)	$D_L$	Ds	$V_L$ (10 <sup>3</sup> ms <sup>-1</sup> )	$V_{S1} = V_{S2}$ (10 <sup>3</sup> ms <sup>-1</sup> )	$V_D$ (10 <sup>3</sup> ms <sup>-1</sup> )
0.74	143.03	407.8	419.19	7.92	4.99	2.48	2.78

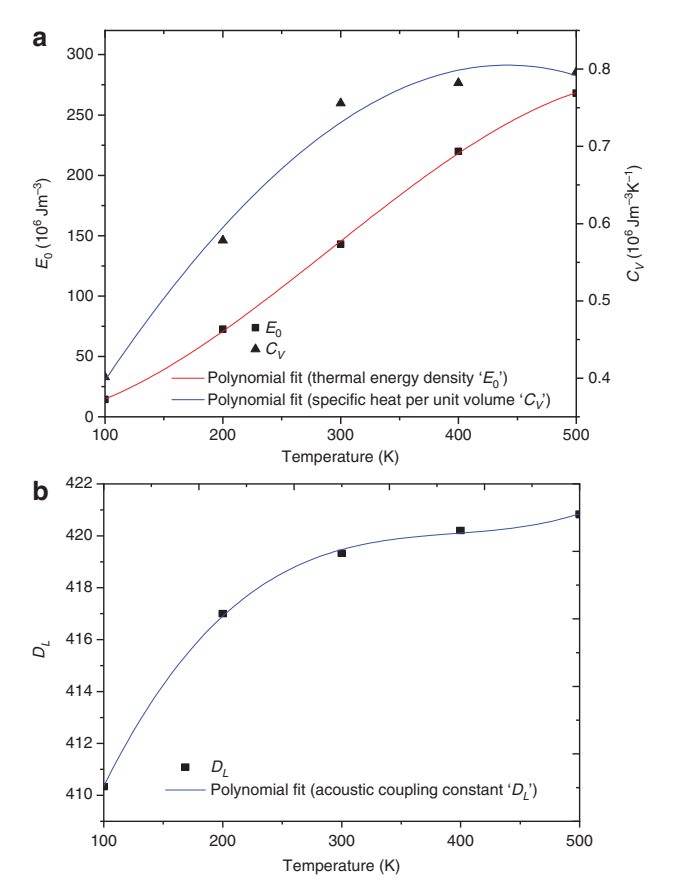


**Figure 3:** (a) Variations of thermal energy density and specific heat per unit volume of the InP-NWs under different temperatures (b) Temperature-dependent acoustic coupling constant of the InP-NWs.

The order of  $\tau$  presented in pico-seconds indicates that the equilibrium distribution of the thermal phonons will be retained within  $\sim \! 10^{-12}$  s. Based on the order of  $\tau$ , we conclude that the WZ-InP-NWs show a semiconducting behavior. The ultrasonic attenuation has been found to increase with an increase in size of nanowires (Tab. 3

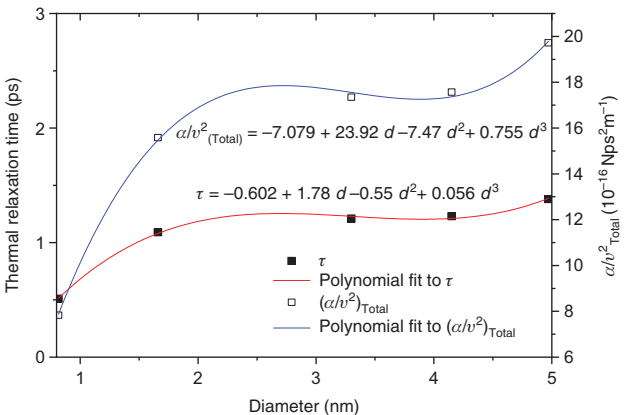
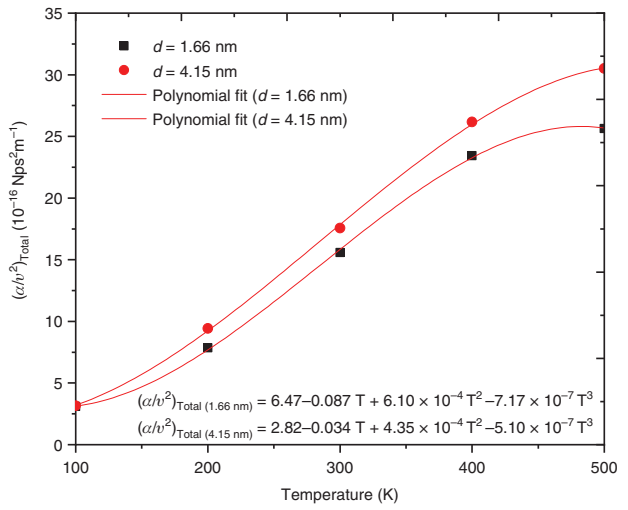


Figure 4: The diameter-dependent au and  $\left(\alpha/\upsilon^2\right)_{\text{Total}}$  at 300 K.



 $\textbf{Figure 5:} \ \ \textbf{The total ultrasonic attenuation with different temperatures.}$ 

and Fig. 4). This feature is due to the incremental variation in the phonon mean free path with an increase in the size of nanowires. Similar characteristics have been also

**Table 3:** The temperature-dependent  $\tau$ ,  $\kappa$ ,  $\left(\alpha/\upsilon^2\right)_{\mathsf{Long.Akh}}$ ,  $\left(\alpha/\upsilon^2\right)_{\mathsf{Shear.Akh}}$ , and  $\left(\alpha/\upsilon^2\right)_{\mathsf{TE}}$  for the InP-NWs with diameters of 1.66 nm and 4.15 nm.

Temp. (K)	τ (ps)	$(Wm^{-1} K^{-1})$	$ig(lpha/arphi^2ig)_{ extsf{Long.Akh}}$ (10 $^{-16}$ Nps $^2$ m $^{-1}$ )	$rac{\left(lpha/arphi^2 ight)_{Shear.Akh}}{\left(10^{-16}\;Nps^2m^{-1} ight)}$	$(\alpha/\upsilon^2)_{TE}$ (10 <sup>-18</sup> Nps <sup>2</sup> m <sup>-1</sup> )
at d = 1.66  nr	n				
100	2.21	2.3	2.86	0.22	0.72
200	1.09	1.92	7.29	0.56	1.21
300	1.09	2.11	14.4	1.11	1.99
400	1.06	2.16	21.7	1.66	2.72
500	0.85	1.77	23.7	1.82	2.79
at $d = 4.15 \text{ nr}$	n				
100	2.26	2.35	2.92	0.22	0.74
200	1.30	2.30	8.73	0.67	1.45
300	1.23	2.38	16.30	1.25	2.25
400	1.19	2.41	24.27	1.85	3.03
500	1.14	2.36	27.72	2.42	3.72

reported in a diameter-dependent study on GaAs-NWs [41]. Figure 4 indicates the characteristics of the thermal relaxation time  $\tau$  and total ultrasonic attenuation  $(\alpha/v^2)_{\text{Total}}$  with respect to the nanowire diameter variation at 300 K. The curve fit equation for  $\tau$  and  $(\alpha/v^2)_{\text{Total}}$  with the nanowire diameter follows the polynomial  $\sum_{i=1}^3 a_i d^i$ . The Akhieser loss for the longitudinal wave  $(\alpha/v^2)_{\text{Long.Akh}}$  is found to be dominant towards the total loss of ultrasonic energy by the InP-NWs. The close similarity between the variation of  $\tau$  and  $(\alpha/v^2)_{\text{Total}}$  with the diameter of the InP-NWs reveals that the diameter dependent variation of the ultrasonic attenuation for the InP-NWs is predominantly affected by its thermal conductivity/thermal relaxation time.

Although the quantities  $\tau$  and  $\kappa$  are slightly large for a large diameter of InP-NWs, they are almost constant under the temperature variation (Tab. 3) while total attenuation is continually increasing with temperature (Fig. 5). Thus, the temperature variation of the total ultrasonic attenuation for InP-nanowire is not affected by  $\tau$  and  $\kappa$ . Instead, the temperature variation affects the thermophysical properties of the material influencing the ultrasonic attenuation as described in (6)–(7). Figure 3 shows that the quantities  $E_0$ ,  $C_V$  and  $D_L$  increase with temperature for the InP-NWs. The thermal energy density  $E_0$  is found to be the governing factor in the temperature variation of the total ultrasonic attenuation of the InP-NWs. Thus, a strong correlation exists between the total ultrasonic attenuation  $(\alpha/v^2)_{Total}$  with thermal energy density  $E_0$  for the InP-NWs at different temperature. The value of  $(\alpha/v^2)_{Total}$  has been found to increase with both diameter and the temperature of the InP-NWs (Figs. 4 and 5). The similar characteristic of ultrasonic attenuation has also been reported for the nanocrystalline PbTe (fcc structure) [34] and Ta (bcc structure) [42]. Thus, the InP-NWs of low diameter will have good energy stability under low temperature.

The cross-sectional view of the WZ-InP-NWs (Fig. 1) clearly indicates that more atoms lie within the volume in comparison to surface. Hence, as the ultrasonic wave propagates through the nanowire, very few interactions of shear phonons with the thermal phonons of the medium occur. However, longitudinal phonons interact in large amounts. As a result, acoustic coupling constants and Akhieser loss for the longitudinal ultrasonic wave propagation will be greater than that of the shear mode, i.e.  $D_L > D_S$  and  $(\alpha/v^2)_{\rm Long.Akh} > (\alpha/v^2)_{\rm Shear.Akh}$ , thus validating our findings depicted in Tables 2 and 3, respectively. Similar characteristics have also been reported in previous studies on similar structured nanowires [33, 34, 38]. Thus, the thermoelastic relaxation process is inferior to the

phonon-phonon interaction process in terms of producing ultrasonic attenuation in the InP-NWs. The values of the ultrasonic attenuation due to the phonon-phonon interaction and the thermoelastic relaxation mechanisms in case of the InP-NWs (Tab. 3) have been found to be less than those of the ZnO-NWs and InN-NWs [18, 33]. This finding indicates that the chosen material, InP, has good applicability for futuristic applications in the industry.

## 4 Conclusion

The findings and discussion elaborated for the WZ-InP-NWs validates our theoretical approach of using the potential model for the estimation of higher order elastic constants and the ultrasonic properties. The nature of the SOECs and TOECs are similar to the other semiconducting nanowires of this group. The mechanical stability criteria described by Born have been satisfied for the WZ-InP-NWs. The ductile nature of the WZ-InP-NWs is also confirmed by Pugh's ratio. The relaxation time observed is in pico-seconds, thus confirming the semiconducting nature of the material. The ultrasonic velocity characteristics reveal that the restoration time of thermal phonon distribution will be least for the wave propagating at an angle 50°.  $(\alpha/\upsilon^2)_{\rm Long.Akh} > (\alpha/\upsilon^2)_{\rm Shear.Akh}$ , thus validating the prominent contribution of the ultrasonic attenuation for the wave propagation along longitudinal mode. It has been also observed that ultrasonic attenuation in the WZ-InP-NWs depends on their size, that is, larger the diameter, larger the attenuation produced in the NWs. The ultrasonic attenuation in the InP-NWs due to size variation is mostly affected by thermal conductivity, whereas its temperature dependency is governed by the thermal energy density.

Our study provides a description of the higher order elastic constants, thermophysical properties, mechanical properties and ultrasonic properties of the WZ-InP-NWs. The obtained results of the present study may be used for further investigations on the WZ-InP-NWs and their applications in nanowire-based devices. Finally, the elastic and thermophysical properties in correlation with the temperature and diameter variations of the nanowires discussed above may be further explored for different industrial applications.

**Acknowledgment:** The authors are highly thankful to the reviewers of the manuscript who have meticulously given their valuable comments for the enrichment of our work.

# References

- [1] K. Ikejiri, Y. Kitauchi, K. Tomioka, J. Motohisa, and T. Fukui, Nano Lett. 11, 4314 (2011).
- [2] Z. Liu, I. Papadimitriou, M. Castillo-Rodríguez, C. Wang, G. Esteban-Manzanares, et al., Nano Lett. 19, 4490 (2019).
- [3] A. Baida and M. Ghezali, Comput. Condens. Matter. 17, e00333 (2018).
- [4] X. Yan, X. Zhang, J. Li, Y. Wu, and X. Ren, Appl. Phys. Lett. 107, 023101 (2015).
- [5] C. Cordoba, X. Zeng, D. Wolf, M. T. Borgström, E. Barrigón, et al., Nano Lett. 19, 3490 (2019).
- [6] J. Wallentin, M. Ek, L. R. Wallenberg, L. Samuelson, and M. T. Borgström, Nano Lett. 12, 151 (2012).
- [7] X. Yan, B. Li, Q. Lin, P. Liu, Y. Luo, et al., Appl. Phys. Lett. 114, 243106 (2019).
- [8] P. Caroff, K. A. Dick, J. Johansson, M. E. Messing, K. Deppert, et al., Nat. Nanotechnol. 4, 50 (2009).
- [9] D. Li, Z. Wang, and F. Gao, Nanotechnology 21, 505709 (2010).
- [10] F. Boxberg, N. Søndergaard, and H. Q. Xu, Adv. Mater. 24, 4692 (2012).
- [11] Y. Kitauchi, Y. Kobayashi, K. Tomioka, S. Hara, K. Hiruma, et al., Nano Lett. 10, 1699 (2010).
- [12] C. L. Dos Santos and P. Piguini, Phys. Rev. B. 81, 075408 (2010).
- [13] M. De Luca and A. Polimeni, Appl. Phys. Rev. 4, 041102 (2017).
- [14] D. Prete, P. A. Erdman, V. Demontis, V. Zannier, D. Ercolani, et al., Nano Lett. 19, 3033 (2019).
- [15] D. J. O. Göransson, M. T. Borgström, Y. Q. Huang, M. E. Messing, D. Hessman, et al., Nano Lett. 19, 2674 (2019).
- [16] D. K. Pandey, D. Singh, and R. R. Yadav, Appl. Acoust. 68, 766
- [17] A. K. Yadav, R. R. Yadav, D. K. Pandey, and D. Singh, Mater. Lett. 62, 3258 (2008).
- [18] S. Tripathi, R. Agarwal, and D. Singh, Johnson Matthey Technol. Rev. 63, 166 (2019).
- [19] M. Born, K. Huang, Dynamical Theory of Crystal Lattices, Clarendon Press, Oxford 1954, p. 420.
- [20] P. F. Weck, E. Kim, V. Tikare, and J. A. Mitchell, Dalton Trans. 44, 18769 (2015).
- [21] H. Qin, X. Luan, C. Feng, D. Yang, and G. Zhang, Materials. 10, 1419 (2017).

- [22] C. P. Yadav, D. K. Pandey, and D. Singh, Indian J. Phys. 93, 1147
- [23] D. K. Pandey and S. Pandey, Acoustic Waves, Tech, Rijeka, Croatia 2010, pp. 398-430.
- [24] W. P. Mason, Physical Acoustics, Vol. III-B, Academic Press Inc., New York 1965, pp. 235-286.
- [25] C. Tripathy, D. Singh, and R. Paikaray, Can. J. Phys. 96, 513 (2018).
- [26] J. Carrete, R. C. Longo, L. M. Varela, J. P. Rino, and L. J. Gallego, Phys. Rev. B. 80, 155408 (2009).
- [27] M. Nandanpawar and S. Rajagopalan, J. Acoust. Soc. Am. 71, 1469 (1982).
- [28] D. E. Gray (Ed.), American Institute of Physics Handbook, 3rd ed. McGraw-Hill, New York 1956, pp. 4-44, 4-57.
- [29] D. Kriegner, E. Wintersberger, K. Kawaguchi, J. Wallentin, M. T. Borgström, et al., Nanotechnology. 22, 425704
- [30] C. Hajlaoui, L. Pedesseau, F. Raouafi, F. B. C. Larbi, J. Even, et al., J. Exp. Theor. Phys. 121, 246 (2015).
- [31] S. Q. Wang and H. Q. Ye, Phys. Stat. Solidi B. 240, 45 (2003).
- [32] S. Ehsanfar, F. Kanjouri, H. Tashakori, and A. Esmailian, J. Electron. Mater. 46, 6214 (2017).
- [33] S. K. Verma, D. K. Pandey, and R. R. Yadav, Physica. B Condens. Matter. 407, 3731 (2012).
- [34] P. K. Dhawan, S. Upadhyay, S. K. Verma, M. Wan, R. R. Yadav, et al., Mater. Lett. 114, 15 (2014).
- [35] M. Dunaevskiy, P. Geydt, E. Lähderanta, P. Alekseev, T. Haggrén, et al., Nano Lett. 17, 3441 (2017).
- [36] H. Cui, Y. Zhang, Q. Kang, H. M. Chang, X. B. Zhang, et al., Optik. 177, 58 (2019).
- [37] S. Mukhopadhyay and D. A. Stewart, Phys. Rev. B, 89, 054302 (2014).
- [38] S. Tripathi, R. Agarwal, and D. Singh, J. Pure Appl. Ultrason. 41, 44 (2019).
- [39] S. Tripathi, R. Agarwal, and D. Singh, Int. J. Thermophys. 40, 78 (2019).
- [40] S. D. Dabhi and P. K. Jha, J. Therm. Anal. Calorim. 124, 1341
- [41] P. K Dhawan, M. Wan, S. K. Verma, D. K. Pandey, and R. R. Yadav, J. Appl. Phys. 117, 074307 (2015).
- [42] R. R. Yadav and D. K. Pandey, Acta Phys. Pol. A, 107, 933 (2005).